Science Bulletin 64 (2019) 764–773

Contents lists available at ScienceDirect

Science Bulletin

journal homepage: www.elsevier.com/locate/scib

Article

In situ redox growth of mesoporous Pd-Cu_2O nanoheterostructures for improved glucose oxidation electrocatalysis

Ying Guo [a,b,1], Jianwen Liu [c,d,1], Yi-Tao Xu [a], Bo Zhao [a], Xuewan Wang [c], Xian-Zhu Fu [a,c,*], Rong Sun [a,*], Ching-Ping Wong [e,f]

[a] Shenzhen Institutes of Advanced Technology, Chinese Academy of Sciences, Shenzhen 518055, China
[b] Department of Materials Science and Engineering, City University of Hong Kong, Hong Kong, China
[c] College of Materials Science and Engineering, Shenzhen University, Shenzhen 518055, China
[d] National Supercomputing Center in Shenzhen, Shenzhen 518055, China
[e] Department of Electronics Engineering, The Chinese University of Hong Kong, Hong Kong, China
[f] School of Materials Science and Engineering, Georgia Institute of Technology, Atlanta, GA 30332, USA

ARTICLE INFO

Article history:
Received 8 February 2019
Received in revised form 21 March 2019
Accepted 10 April 2019
Available online 17 April 2019

Keywords:
Metal-oxide interfaces
Crystalline defects
Interfacial electron accumulation
Electrocatalysts
Density functional theory

ABSTRACT

Interfaces of metal-oxide heterostructured electrocatalyst are critical to their catalytic activities due to the significant interfacial effects. However, there are still obscurities in the essence of interfacial effects caused by crystalline defects and mismatch of electronic structure at metal-oxide nanojunctions. To deeply understand the interfacial effects, we engineered crystalline-defect Pd-Cu_2O interfaces through non-epitaxial growth by a facile redox route. The Pd-Cu_2O nanoheterostructures exhibit much higher electrocatalytic activity toward glucose oxidation than their single counterparts and their physical mixture, which makes it have a promising potential for practical application of glucose biosensors. Experimental study and density functional theory (DFT) calculations demonstrated that the interfacial electron accumulation and the shifting up of *d* bands center of Cu-Pd toward the Fermi level were responsible for excellent electrocatalytic activity. Further study found that Pd(3 1 0) facets exert a strong metal-oxide interface interaction with Cu_2O(1 1 1) facets due to their lattice mismatch. This leads to the sinking of O atoms and protruding of Cu atoms of Cu_2O, and the Pd crystalline defects, further resulting in electron accumulation at the interface and the shifting up of *d* bands center of Cu-Pd, which is different from previously reported charge transfer between the interfaces. Our findings could contribute to design and development of advanced metal-oxide heterostructured electrocatalysts.

1. Introduction

Efficient catalyst is indispensable for the electrochemical oxidation of glucose, which has wide applications in biosensors and full cells [1,2]. Noble metals are traditional electro-catalysts for oxidation of organics including glucose [3–5], however, they are usually high cost, low selectivity, and easily poisoned by the intermediates formed during organics oxidation [6]. Although, metal oxide electrocatalysts (Cu_2O, CuO, Co_3O_4, NiO, TiO_2, etc.) are promising candidates for glucose oxidation because of their low cost, excellent anti-interference and anti-poisoning towards interfering species [7–11]. Unfortunately, the metal oxides usually suffer from still unsatisfactory electrocatalytic activity and relatively low conductivity [12].

Metal-oxide heterostructured catalysts combining the advantages of metals and oxides usually achieve much higher performance than their single counterparts or physical mixture [13–16]. Those excellent catalytic activities are attributed to the interfacial effects of the strong metal-support interactions (SMSI) [17–22]. Tremendous efforts have been devoted to this issue since the concept of SMSI was first proposed for catalysis in 1978 [23–28]. It was further found that electron transfer and oxygen vacancy were responsible for SMSI, which were proposed to be caused by the work function discrepancy of the two components and the oxygen transfer from oxide to metal, respectively [29–31]. Consequently, more active sites were produced for the improved catalytic performance of metal-oxide heterostructures [32–34]. Nowadays, this has been well known and been employed to design various metal-oxide heterostructured catalysts with good activity, selectivity and stability [35–37].

Until now, the energetic, electronic and geometric properties of metal and oxide supports have been mainly investigated to

* Corresponding authors.
E-mail addresses: xz.fu@szu.edu.cn (X.-Z. Fu), rong.sun@siat.ac.cn (R. Sun).
[1] Ying Guo and Jianwen Liu contributed equally to this work.

https://doi.org/10.1016/j.scib.2019.04.025
2095-9273/

elucidate the SMSI effect, but it has not reached an agreement on SMSI. Because of the different lattice parameters between metal and oxide support (especially lattice mismatch over 3%) [38], SMSI effects will lead to their crystal structure changes at the interfaces, which results in remarkable crystalline defects [39,40]. Such imperfect lattice could facilitate the catalytic chemical bond breaking of the targeted substrates [40,41]. Although the influences of atomic rearrangement and crystalline defects on the electrocatalytic activity of heterostructured catalysts have been mentioned in several cases, there is rare experimental and theoretical support [32,40]. Moreover, the interfacial charge state also strongly depends on the crystal structures of metal and oxide nanojunction. Therefore, the imperfect crystalline feature of the nanojunction always comes along with their electronic structure change. Such specific interfacial effects may give rise to new or improved catalytic activity. Recently, suppressed electron transfer phenomenon was found by Pt nucleation at defect sites of CeO_2 [27]. However, the effect of crystalline defects on electronic structure and catalytic performance of metal-oxide nanojunction needs to be investigated in detail.

To address this challenge, we engineered Pd-Cu_2O nanoheterostructures with large lattice mismatch of 8.68% as a model to study their electrocatalytic activity towards glucose oxidation. Experimental characterization demonstrated the interfacial interaction between Pd(3 1 0) and Cu_2O(1 1 1) facets, which play a crucial role on the improvement of electrocatalytic activity. Different from previously reported electron transfer [29,32,35], further study showed that the metal atom dislocation and defects lead to electron accumulation at the interface and the shifting up of *d* bands center of Cu-Pd toward the Fermi level, and eventually enhance the activity of Pd-Cu_2O nanoheterostructures to expedite the electrochemical glucose oxidation [40,42].

2. Experimental

2.1. Materials, preparation, and characterization

2.1.1. Materials

All chemical reagents were analytical grade and used without further purification. Palladium chloride ($PdCl_2$, ≥99.9%), copper chloride dehydrate ($CuCl_2{\cdot}2H_2O$, ≥99.0%), hydrazine ($N_2H_4{\cdot}H_2O$, 85%), polyvinylpyrrolidone (PVP, K-30), potassium hydroxide (KOH, ≥90%), hydrochloric acid (HCl, 37%), glucose ($C_6H_{12}O_6$, ≥99.8%), uric acid ($C_5H_4N_4O_3$, ≥99.0%), sodium chloride (NaCl, ≥99.5%), dopamine hydrochloride ($C_8H_{11}NO_2{\cdot}HCl$) and ascorbic acid ($C_6H_8O_6$, ≥99.7%) were purchased from Sinopharm Chemical Reagent Co., Ltd. (China). High purity N_2 was supplied by the Shenzhen Hongzhou Industrial Gases Co., Ltd. (China). Deionized Mini-Q water (18 MΩ cm) was used for all experiments.

2.1.2. Synthesis of mesoporous Cu_2O nanoparticles

A 20 μL of $N_2H_4{\cdot}H_2O$ (85%) was injected into 100 mL mixed aqueous solution that contained $CuCl_2$ (1 mmol/L) and PVP (2 mmol/L) under constant stirring at room temperature. After reaction for 5 min, the final precipitates were extracted from the solution by centrifugation, and then washed with distilled water and ethanol for 5 times, dried in vacuum at 40 °C for 4 h.

2.1.3. Synthesis of mesoporous Pd-Cu_2O nanoheterostructures

A 10 mmol/L H_2PdCl_4 aqueous solution was firstly prepared by completely dissolved 88.6 mg $PdCl_2$ in 50 mL of 20 mmol/L HCl under ultrasonic treatment 30 min. A 0.5 mL 10 mmol/L H_2PdCl_4 aqueous solution was rapidly injected into 100 mL of the above resulting Cu_2O colloid, and the aqueous solution immediately turned into dark green. After 10 min, the obtained solution was centrifuged and the precipitate were washed with deionized water and ethanol for 5 times then dried in vacuum at 40 °C for 4 h. In addition, Pd-Cu_2O-10 nanoheterostructures and Pd-Cu_2O-80 nanoheterostructures were also prepared as the control samples using the same procedure through adding 1 and 0.125 mL 10 mmol/L H_2PdCl_4 solution, respectively.

2.1.4. Synthesis of Pd nanoparticles

A 100 mL mixed solution containing H_2PdCl_4 (0.5 mmol/L) and PVP (1 mmol/L) was stirred for 5 min under room temperature. And then 10 mL 0.1 mol/L $NaBH_4$ aqueous solution was immediately added to the mixture under vigorous stirring. The obtained solution was centrifuged and the particles were washed with deionized water and ethanol for 5 times then dried in vacuum at 40 °C for 4 h.

2.1.5. Synthesis of Pd-Cu_2O mixtures by impregnation method

Mesoporous Pd-Cu_2O composite catalysts prepared by impregnation method. A 10 mL of the as-synthesized Pd colloid was added to 50 mL of the above Cu_2O colloid, then the mixtures was stirred for 10 min. The solution was centrifuged and the particles were washed with deionized water and ethanol for 5 times then dried in vacuum at 40 °C for 4 h.

2.1.6. Characterization

The morphologies and structures of as-synthesized nanoparticles were characterized by field emission scanning electron microscopy (FE-SEM, FEI Nova Nano SEM 450, USA) and high resolution transmission electron microscopy (HRTEM, Tecnai G2 F20 FEI, USA), respectively. The X-Ray diffraction (XRD, Rigaku D/Max 2500, Japan) with Cu Kα radiation was taken to measure the crystallographic structure of the as-prepared samples. The electrochemical measurements were carried out on electrochemical workstation (CHI 660E, China).The XPS data were gained from PHI-1800 X-ray photoelectron spectra spectrometer (XPS, PHI-1800, Japan). The ultraviolet–visible spectroscopy (UV–Vis) spectra of as-prepared samples in ethanol were measured on UV–Vis-NIR spectrometer (Shimadzu UV-3600, Japan) with a wavelength range of 250–800 nm.

2.2. Electrochemical preparation

The drop-casting films of the synthesized samples on a glassy carbon electrode (GCE, diameter: 5 mm, area: 0.196 cm^2) were used as the working electrode. The saturated calomel electrode (SCE) and the platinum-plate electrode (1 cm × 1 cm) were served as the reference electrode and the counter electrode, respectively. Prior to electrochemical measurements, the GCE was polished with 50 nm α-Al_2O_3 powder to a high mirror finish and cleansed by sonication. The catalysts inks were prepared by dispersing the as-synthesized catalysts (1.6 mg) in deionized water (1 mL), ethanol (2.5 mL) and 0.1 wt% Nafion (0.5 mL). The dispersion was sonicated for 30 min to form a homogeneous ink. And then as-synthesized samples solution (10 μL) was deposited on the GCE and dried at 40 °C. This procedure was repeated 5 times so that a total amount of 50 μL catalysts ink were loaded on electrode, with a sample loading of 20 μg, then dried. Next, 10 μL 0.1 wt% Nafion solution was dropped on the surface of the above catalysts modified CGE and dried at 40 °C before electrochemical experiments.

All electrochemical measurements were carried out in N_2-saturated 0.1 mol/L KOH solution. A conventional three-electrode cell system was conducted at room temperature. The drop-casting films of the synthesized samples on GCE were used as the working electrode. The SCE and the platinum-plate (1 cm × 1 cm) electrode were served as the reference electrode

and the counter electrode, respectively. The cyclic voltammograms (CVs) were recorded at a scan rate of 100 mV/s from −0.6 to 0.65 V. The amperometric responses were recorded at 0.5 V. Other electrochemical measurements are available in the Supporting Information (online).

2.3. DFT calculations

The density functional calculations were performed with the Vienna ab initio simulation package (VASP). The projector augmented wave (PAW) method was used to describe the electron–ion interaction. All calculations were performed on periodically repeated slabs using the Perdew-Burke-Ernzerhof (PBE) exchange–correlation functional. The modeling details and relevant references are given in the Supporting Information (online).

3. Results and discussion

3.1. Construction and investigation of crystalline-defect Pd-Cu_2O interfaces

The mesoporous Cu_2O colloids are firstly synthesized by a reducing precipitation reaction of Cu^{2+} ions and $N_2H_4{\cdot}H_2O$ in solution with PVP surfactant at room temperature. Then the mesoporous Cu_2O supported Pd nanoheterostructures are fabricated by the redox reaction of Pd^{2+} ions and mesoporous Cu_2O colloids ($Pd^{2+} + Cu_2O + 2H^+ \rightarrow Pd + 2Cu^{2+} + H_2O$)[43]. The representative morphologies of as-prepared mesoporous Cu_2O particles and Pd-Cu_2O nanoheterostructures are shown in Fig. 1. The uniform Cu_2O spherical particles are about 120 ± 20 nm in diameter and constructed by smaller nanocrystals to form hierarchical structures with mesopores (Fig. 1a–c). During the preparation, numerous Cu_2O nanocrystals would initially nucleate from solution via the rapid reaction between Cu^{2+} ions and N_2H_4 and form orange color colloids (Fig. 1a). The very small Cu_2O nanocrystals with high surface energy would self-assemble into hierarchical Cu_2O porous particles with larger size to reduce the surface energy and prevent the further aggregation. The mesoporous network interior structures of Cu_2O particles are also obviously observed in high magnification SEM and TEM results (Fig. 1b and c). After the addition of H_2PdCl_4 solution into Cu_2O colloid, the color immediately changes to brown green for the formation of Pd-Cu_2O nanoheterostructures (Fig. 1d). The mesoporous Pd-Cu_2O nanoheterostructures are similar to mesoporous Cu_2O particles in shape but with smaller particle size about 80 ± 10 nm and rougher surfaces (Fig. 1d–f). The very fine white (SEM image) or black (TEM image) dots are obviously observed on the surface of the Pd-Cu_2O nanoheterostructures (Fig. 1e, f). Fig. 1f illustrates that the Pd nanoparticles with size of about 5 nm are distributed over the entire surface of mesoporous Cu_2O particles. Oxidative Pd^{2+} ions can etch Cu_2O solid to form Cu^{2+} ions and metallic Pd nanoparticles due to the different reducing potential between Cu_2O/Cu^{2+} (0.203 V) and Pd^{2+}/Pd (0.987 V) [44]. As some Cu_2O crystallites are dissolved by Pd^{2+} ions into solution, the Pd metallic atoms simultaneously grow and anchor on the freshly exposed surface of Cu_2O colloids which served as both reducing agent and support at the high ratio of Cu_2O:Pd^{2+} ions. In addition, the surfaces become rough and the particle sizes become smaller after metallic Pd deposition on the surface of mesoporous Cu_2O particles.

N_2 adsorption-desorption measurements (Fig. 2) further demonstrate that Brunauer-Emmett-Teller (BET) surface area (32.82 m^2/g) of Pd-Cu_2O nanoheterostructures is significantly larger than the original mesoporous Cu_2O particles (17.86 m^2/g) because of the redox etching reaction at the Cu_2O surface. Besides, XRD, STEM-EELS (EELS: electron energy loss spectroscopy) mapping and overview EDX mapping results also confirm metallic Pd (Figs. 3, S1 and S2 (online)) and show the uniform distribution of Pd element on the outer surface of Cu_2O particles, corresponding to SEM/TEM observation (Fig. 4a and b). As a result, the Pd-Cu_2O

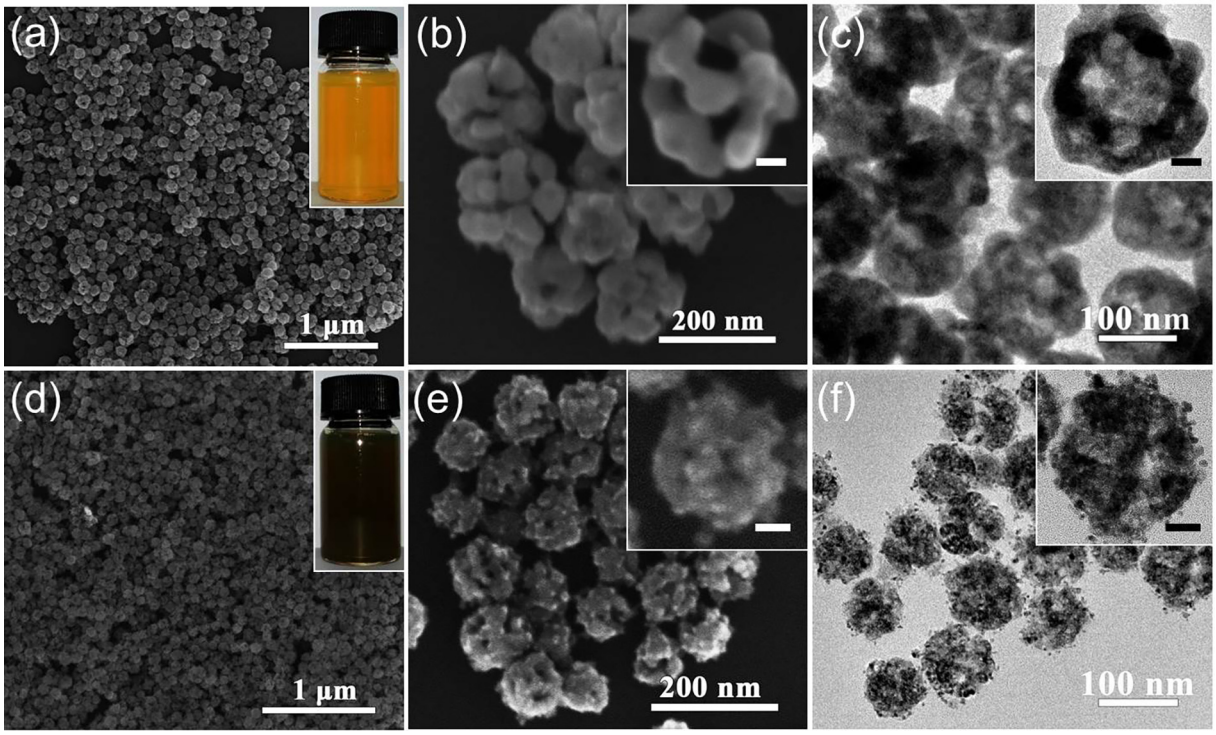

Fig. 1. (Color online) SEM image (a), the high-magnification SEM image (b) and TEM image (c) of Cu_2O nanoparticles. SEM image (d), the high-magnification SEM image (e) and TEM image (f) of Pd-Cu_2O nanoheterostructures. Morphology analysis reveals mesoporous structure, rougher surface and in-situ deposition of Pd on Cu_2O. Scale bars of insets are 25 nm.

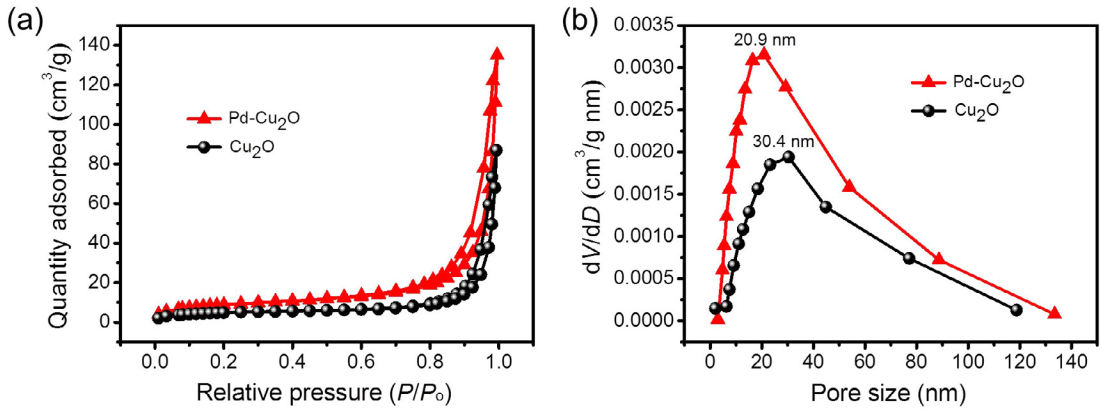

Fig. 2. (Color online) N_2 adsorption/desorption isotherm curve (a) and the corresponding pore sizes distribution (b) of the as-prepared mesoporous Cu_2O nanoparticles and the mesoporous Pd-Cu_2O nanoheterostructures.

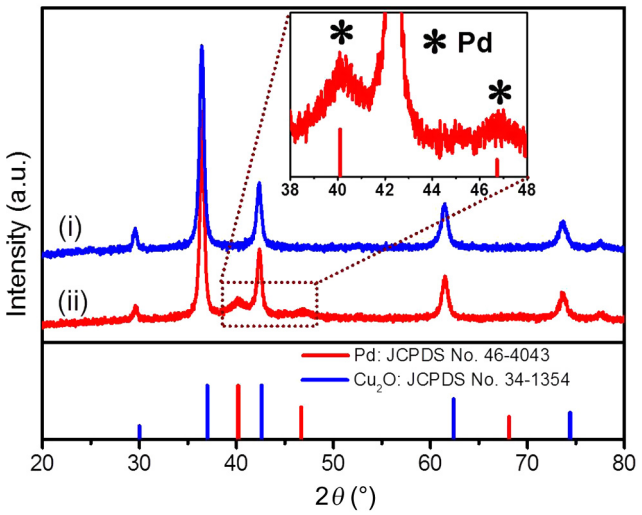

Fig. 3. (Color online) XRD patterns of the obtained samples: Cu_2O nanoparticles (i) and Pd-Cu_2O nanoheterostructures (ii).

interfaces are successfully engineered by deposition of Pd nanocrystals onto the freshly exposed Cu_2O surface. This metal-oxide interface possibly exhibits stronger interfacial interaction between Pd and Cu_2O for the in-situ redox deposition than the interaction derived from the physical mixture method.

The Pd-Cu_2O nanojunction is clearly shown in Fig. 4a. The lattice fringes of Cu_2O(1 1 1) facets do not extend across the interface between Pd and Cu_2O, suggesting that the disordered Pd nanocrystals only non-epitaxially deposit on Cu_2O surfaces for the large lattice mismatch of 8.68% (cell parameter: Pd 3.89 Å, Cu_2O 4.26 Å; lattice mismatch: 8.68%), because the tolerable lattice mismatch for epitaxial growth is generally less than 3% [38]. The SAED patterns of Cu_2O and Pd (Fig. 2a insets) agree with the face-centered cubic (fcc) crystalline of Cu_2O and Pd. The lattice fringes of (1 1 1) facets are not coherently extended across the interface between Cu_2O and Pd nanoparticle. Most importantly, according to the observation of HRTEM in Fig. 4b, we can identify the initially monolayer Pd as (3 1 0) facets as junction facet with Cu_2O(1 1 1) surface. On the other hand, the atom vacancy and edge dislocation (closed by the dotted oval ring and rectangle) are clearly observed at the nanojunction (Fig. 4b). These crystalline defects are ascribed to the large lattice mismatch that can cause serious lattice distortions and/or defects to facilitate the formation of stable interfacial bonds between Pd and Cu_2O [40]. The single Cu atom (circled by the solid ring in Fig. 4b) slightly deviate toward Pd from original position or Cu_2O(1 1 1) crystal facet, so does Pd atom (circled by the dotted ring in Fig. 4b). This directly demonstrates the interfacial atomic rearrangement at the Pd-Cu_2O nanojunction because of the strong interaction between Pd and Cu_2O. The crystalline-defect Pd-Cu_2O interfaces are eventually engineered by taking the large discrepancies of lattice parameters of Pd and Cu_2O.

XPS analysis is further performed to investigate the metal-oxide interaction and chemical state of Pd, Cu, and O. Comparing with

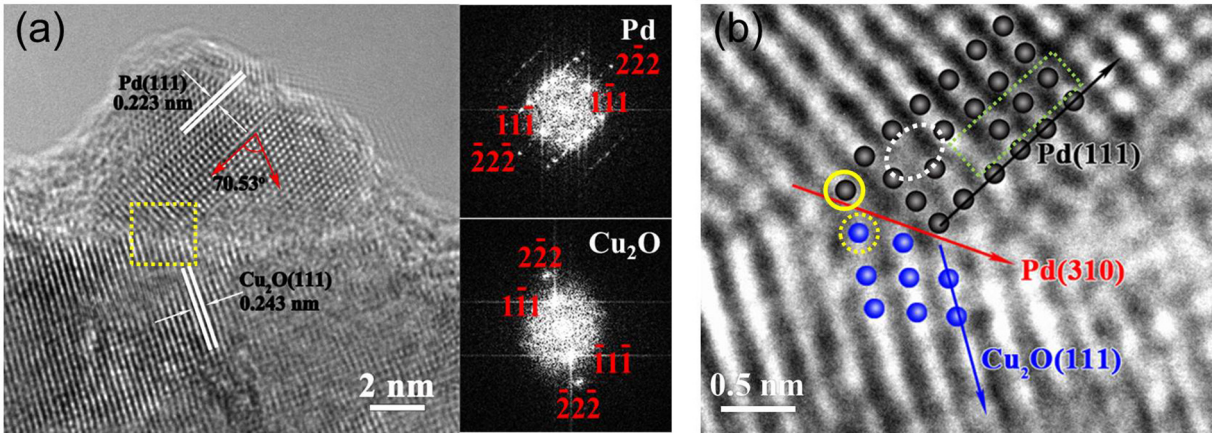

Fig. 4. (Color online) Construction and investigation of Pd-Cu_2O interfaces. (a) HRTEM image taken from Pd-Cu_2O interface and the selected-area electron diffraction (SAED) pattern. (b) The amplification region enclosed with dotted square in (a).

Cu_2O nanoparticles, Cu $2p_{3/2}$ binding energies of Pd-Cu_2O nanoheterostructures are slightly shifted toward higher (0.6 eV) after Pd deposition on the Cu_2O surface (Fig. 5), implying that a strong interaction between Pd and Cu_2O is responsible for charge transfer from Pd to interfaces of Pd(3 1 0)-Cu_2O(1 1 1). However, the binding energy shift is not observed for Pd-Cu_2O physical mixtures obtaining by conventional impregnation method (Fig. 5). It shows that the physical impregnation is not reliable method to achieve strong interaction for electron transfer owing to no chemical bond formation between Pd and Cu_2O. To further confirm the interface interaction, the surface electron states are inspected by high-resolution XPS analysis (Fig. 6 and Table 1). The atomic ration of surface Cu(I):Cu(II) and Pd(0):Pd(II) of Pd-Cu_2O nanoheterostructures are much less than that of the Cu_2O particles, Pd-Cu_2O physical mixtures and Pd nanoparticles, respectively, suggesting that the strong interfacial interaction is responsible for changing the surface atom chemical state at nanojunction. Moreover, the blue-shifted peak of UV–Vis spectra also confirm electron transfer for Pd-Cu_2O nanoheterostructures (Fig. S3 online).

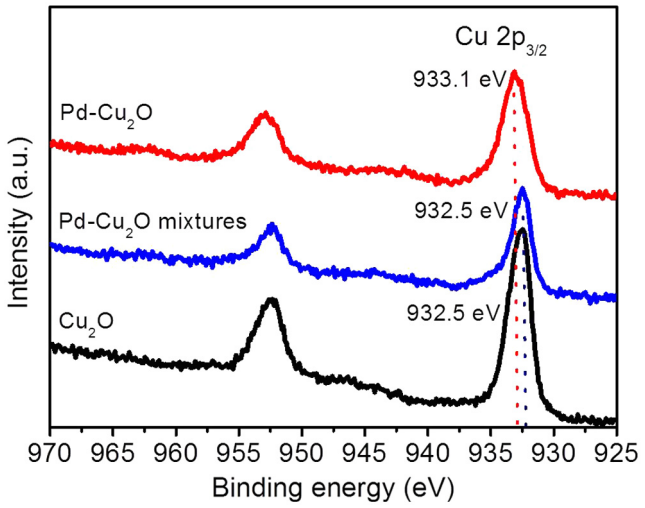

Fig. 5. (Color online) Cu $2p_{3/2}$ XPS spectra of Pd-Cu_2O nanoheterostructures, Pd-Cu_2O mixtures, Cu_2O nanoparticles, and Pd nanoparticles. The binding energies of Cu in Pd-Cu_2O nanoparticles are slightly shifted comparing with other products.

Table 1
Details of surface electron state of as-prepared products derived from XPS spectra.

	Cu(I):Cu(II)	Pd(0):Pd(II)
Pd-Cu_2O	83.0:17.0	69.1:30.9
Pd-Cu_2O mixtures	87.0:13.0	85.0:15.0
Cu_2O	88.8:11.2	–
Pd	–	85.3:14.7

3.2. Electrocatalytic activity of the Pd-Cu_2O nanoheterostructures

As typical CV curves shown in Fig. 7a, Pd-Cu_2O nanoheterostructures display larger current and more negative onset potential than Pd-Cu_2O-10 nanoheterostructures (Fig. S4 online), Pd-Cu_2O-80 nanoheterostructures (Fig. S5 online), Cu_2O nanoparticles and Pd nanoparticles toward glucose oxidation, thus superior electrocatalytic activity. Moreover, Pd-Cu_2O nanoheterostructures exhibit larger successive oxidation current than their counterparts (Fig. 7b, c and Fig. S6 (online)). The sensitivity of Pd-Cu_2O nanoheterostructures is 1.395 mA/(cm^2 mmol/L), which is much higher than that of Pd-Cu_2O-10 nanoheterostructures (1.095 mA/(cm^2 mmol/L)), Pd-Cu_2O-80 nanoheterostructures (1.078 mA/(cm^2 mmol/L)), Cu_2O nanoparticles (0.480 mA/(cm^2 mmol/L)) and Pd nanoparticles (0.042 mA/(cm^2 mmol/L)) (Fig. 7d). In consideration of effect of the interfacial interaction on electrocatalytic activity, Pd-Cu_2O physical mixture is also used as comparison. Expectedly, the oxidation currents and sensitivity of Pd-Cu_2O mixtures are far less than that of Pd-Cu_2O nanoheterostructures (Fig. 7a and d), suggesting that Pd-Cu_2O mixtures do not exhibit the obviously enhanced catalytic activity owing to lack of strong interfacial interaction. Obviously,

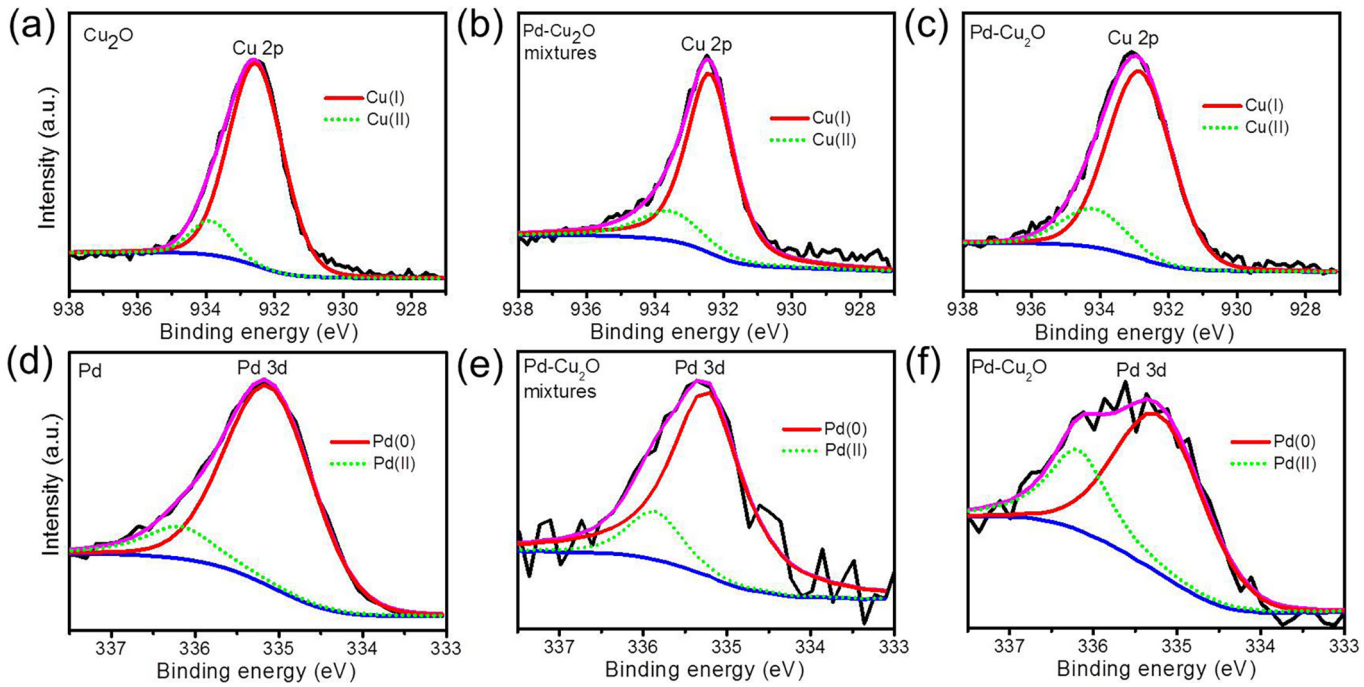

Fig. 6. (Color online) The high-resolution XPS spectra of the as prepared Pd-Cu_2O nanoheterostructures, Cu_2O nanoparticles, and Pd-Cu_2O mixtures and Pd nanoparticles. (a–c) Cu 2p spectrum, (d–f) Pd 3d spectrum.

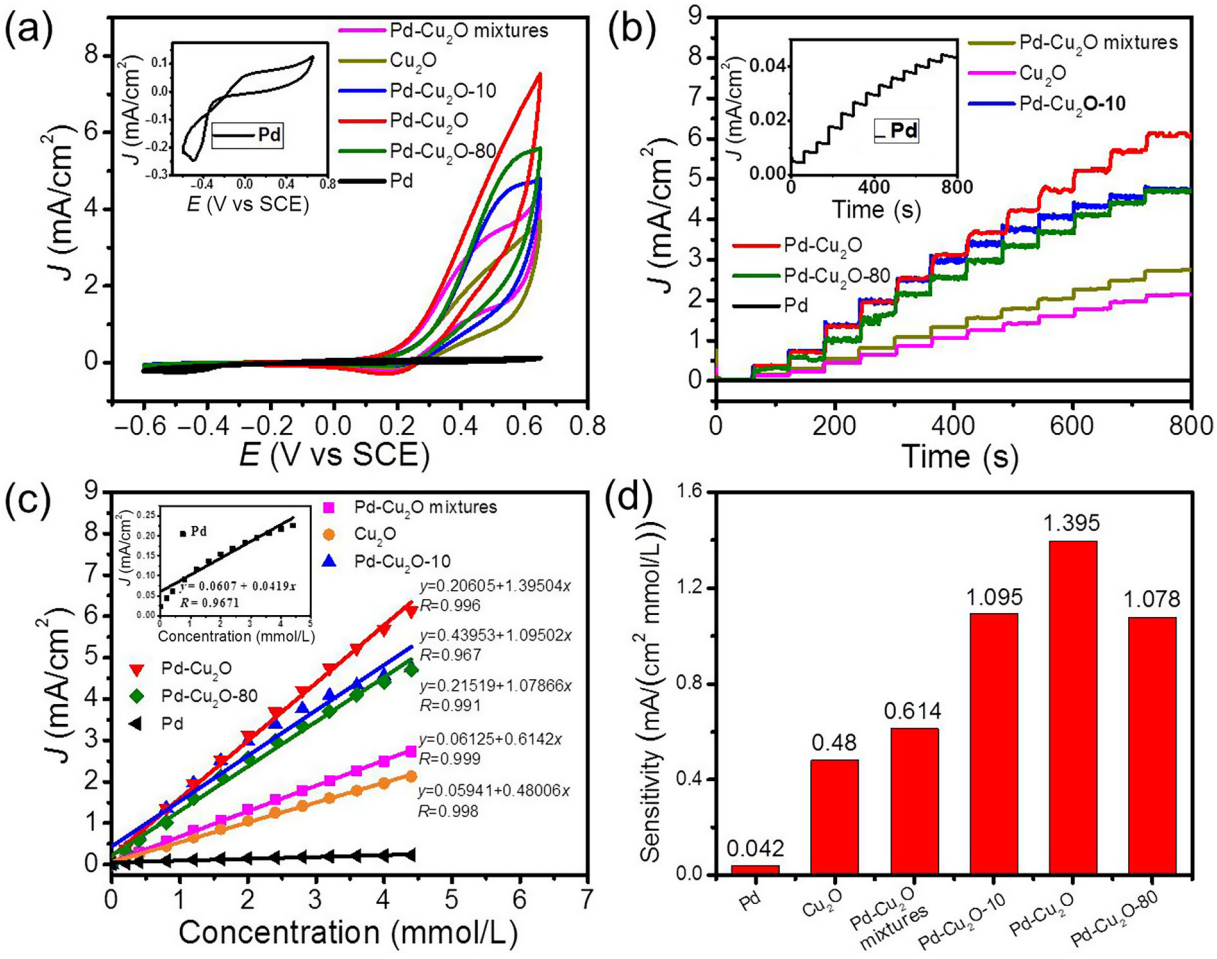

Fig. 7. (Color online) The effect of crystalline-defect interfaces on the catalytic activity of the as-prepared nanoheterostructures was investigated by electrochemical glucose oxidation. (a) CV curves of the modified electrodes in N_2-saturated 0.1 mol/L KOH solution with 4 mmol/L glucose. (b) Amperometic response of the modified electrodes in N_2-saturated 0.1 mol/L KOH solution with the presence of glucose. (c) The corresponding calibration curves of the electrodes. (d) The corresponding sensitivities of the electrodes at a potential of 0.5 V. Inset: the corresponding electrochemical performance curves of Pd nanoparticles.

crystalline defects (vacancies and edge dislocations) and strong interaction at Pd-Cu_2O interfaces of Pd-Cu_2O nanoheterostructures play a critical role in enhancing electrocatalytic activity.

In practical application, the selectivity is an important factor to evaluate the electrocatalytic performance of biosensors because the glucose detection might be interfered by the other chemicals such as ascorbic acid (AA), dopamine (DA), uric acid (UA) and NaCl, which co-exist with glucose in human blood serum [45,46]. It should be noted that the normal physiological level of these species (0.1 mmol/L) is much lower than the glucose. The influence of the above interferents is investigated by amperometric measurements at different potentials (Fig. 8a and Table S1 (online)). During the test, 0.1 mmol/L different interfering species are added into 0.1 mol/L KOH electrolyte containing 1 mmol/L glucose. The signal changes at lower potentials (0.4 and 0.5 V) can be neglected comparing to that from glucose oxidation. At 0.6 V, the current response from the interferents is below 3.5%. Further, the addition of NaCl does not show any effect on the current of glucose oxidation although the chloride ions are easily to poison the sensitivity and efficiency for noble metal glucose sensors. The charge rearrange of nanoheterstructures from Cu_2O might improve the chloride ions poisoning resistance of Pd nanoparticles. The above results indicate that the Pd-Cu_2O nanoheterostructures have excellent selectivity and high chloride tolerance. Electrochemical oxidation of glucose is a kinetically controlled sluggish reaction, which could be improved by the electron interaction in the interface of nanoheterostructure and nanoscopic electrochemical active surface area. Whereas, it is a diffusion-controlled electrochemical reaction for oxidation of AA, UA and AA. The currents of interferents are proportional to the apparent geometric area, regardless of the mesoporous roughness of the catalysts. The most of electroactive interferences in the blood do not show noticeable responsive currents at lower potential for the increased roughness factor on the electrode surface.

The reproducibility and repeatability of the biosensors are performed by a series of 6 assaying sensors prepared in the same condition. The relative standard deviation (R.S.D) of 4.3% is obtained towards 0.3 mmol/L glucose (Fig. 8b), and the 5 successive measurements of a single sensor for 0.3 mmol/L glucose reveal a R.S.D of 5.1% (Fig. 8c), suggesting the good reliability of the method. The biosensor based on Pd-Cu_2O nanoheterostructures still remain high sensitivity of 96.2% the initial response after 30 d, implying the excellent long-term stability (Figs. 8d and S7 (online)), which is suitable for repeating and long duration applications. To further demonstrate the feasibility of the prepared biosensors in practical analysis, it is applied to detect glucose in human blood serum. A serum sample of 80 μL is added in 20 mL of KOH solution before the measurements, and each sample is analyzed using a standard addition method with three times addition of a standard glucose solution. The corresponding results in Table S2 (online) indicate the excellent recoveries of sensors, suggesting that the proposed Pd-Cu_2O nanoheterostructured electrocatalysts may have a promis-

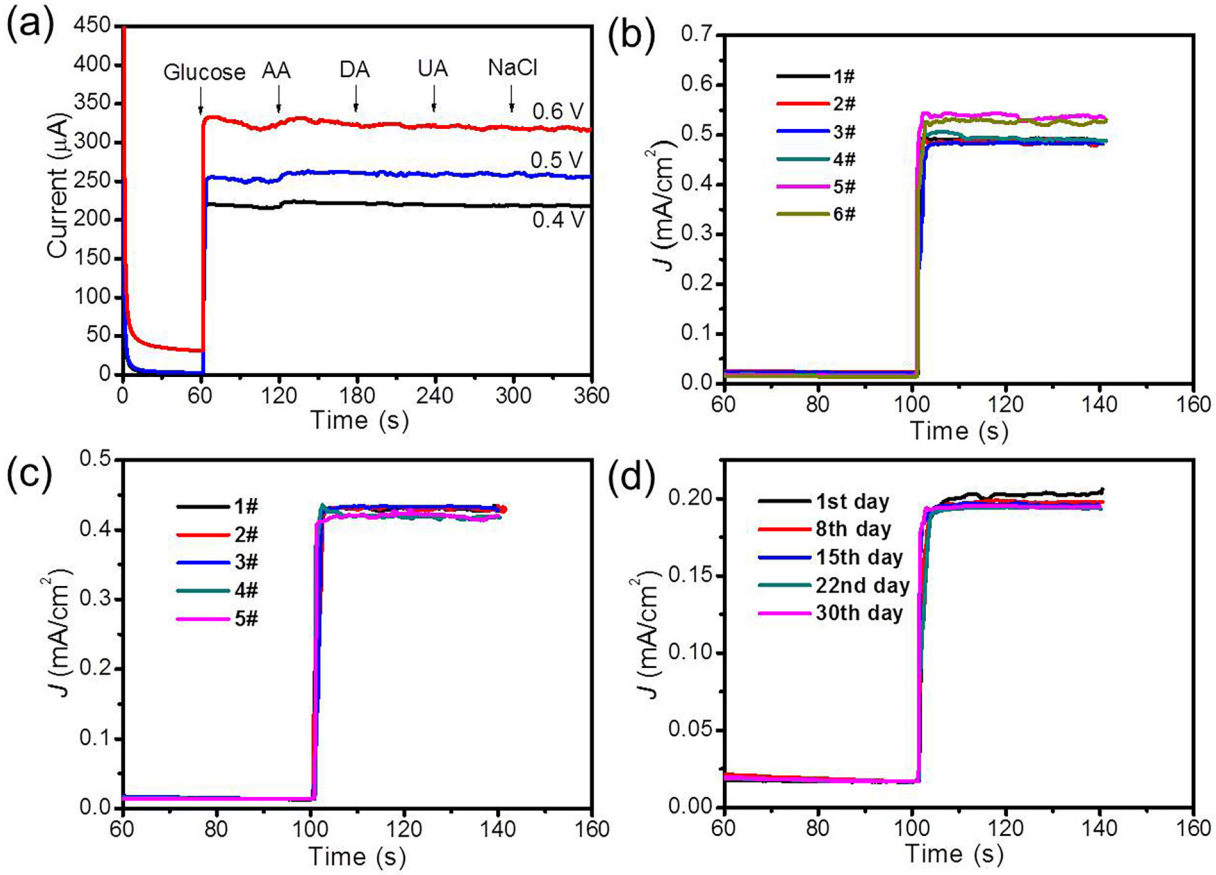

Fig. 8. (Color online) (a) Amperometric response of the sensor to successive additions of 1 mmol/L glucose, 0.1 mmol/L interferents in N_2-saturated 0.1 mol/L KOH solution at 0.5, 0.6 and 0.7 V. (b) The reproducibility of the sensor is performed by a series of 6 assaying sensors prepared in the same condition. (c) The repeatability of the sensor is measured by the 5 successive measurements of a singer sensor in N_2-saturated 0.1 mol/L KOH at 0.5 V. (d) The aging tolerance of the prepared sensor over 30 d storage period.

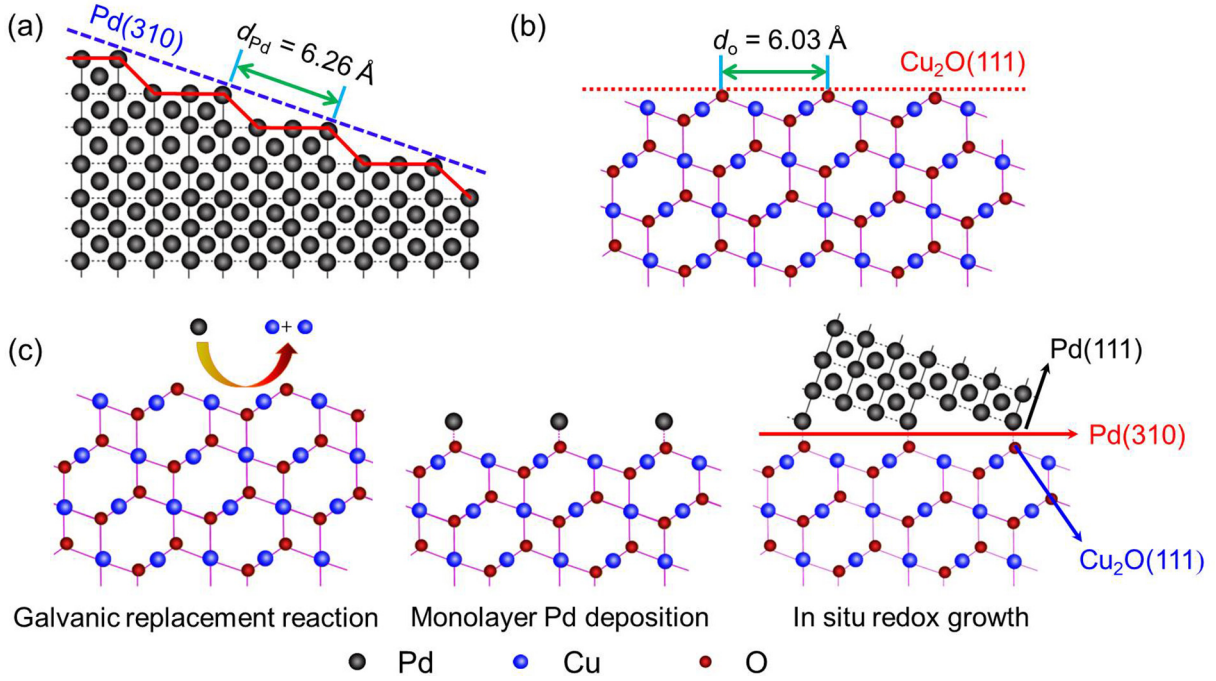

Fig. 9. (Color online) (a) Pd atomic model of the (3 1 0) plane projected along the ⟨0 0 1⟩ axis. The dotted line represents Pd (3 1 0) facets. (b) Cu_2O atomic model (side view) of the (1 1 1) plane. (c) Redox non-epitaxial growth mechanism of Pd-Cu_2O nanoheterostructures.

ing potential for practical application for glucose oxidation and detection. Besides, the morphology and composition of Pd-Cu_2O nanoheterostructures are also investigated after the CV test for 100 cycles in N_2-saturated 0.1 mol/L KOH solution with 4 mmol/L glucose. The results show the rough surface is well-preserved Fig. S8 (online), which is consistent with the original morphology (Fig. 1e), and the atomic ratio of Pd is slightly decreased.

3.3. DFT calculations on Pd-Cu_2O nanoheterostructures

The DFT calculations are used to further explore the effects of Pd-Cu_2O interfaces in essence. As the HRTEM provide clear hints that Pd(3 1 0) facet grows on the Cu_2O(1 1 1) facet in Fig. 4d, the facets interfacing deduction for Pd(3 1 0) and Cu_2O(1 1 1) is performed to uncover the underlying pattern (Section 4 of Supporting Information online). The mathematical deduction result shows junction of these two facets, although the surface Pd distances for the (3 1 0) facet is 6.26 Å, around 8.66% larger than that for surface dangling O atoms distances (d_O = 6.03 Å) on the Cu_2O(1 1 1) surface as shown in Fig. 9a and b. Because the facets do not match perfectly, periodic model for Pd(3 1 0) growth on the Cu_2O(1 1 1) is not practical. Instead, Pd cluster models are built to simulate the Pd (3 1 0) growth on Cu_2O(1 1 1) facet (Fig. 9c) as Pd cluster model can also preserve the facet ideally based on our calculations (Figs. S9 and S10 online). The Pd_{47} and Pd_{46} clusters are built to model the ideal Pd(3 1 0) facet and Pd(3 1 0) facet with a vacancy (Fig. S11 online).

Fig. 10a and b shows the optimized structures for Pd_{47} and Pd_{46} cluster in facet (3 1 0) junction with Cu_2O(1 1 1). Although differing only one vacancy, the interface of Pd_{46}-Cu_2O shows much more chemical bonds than that for Pd_{47}-Cu_2O. The reason is attribute to the lattice parameter mismatching of Pd(3 1 0) and Cu_2O(1 1 1), which introduces the strain at the interface of Pd(3 1 0) and Cu_2O (1 1 1), resulting in the sinking of the O atoms and protruding of Cu atoms. The introduced vacancy hereby lessens the strain stress to strengthen interfacial bonds formation. It excellently bears out experimental observation on Cu deviation as shown in Fig. 4d. As a result of the interfacial Pd-O and Pd-Cu bonds formation, the electron accumulation is discovered at the interface of Pd-Cu_2O as shown in the differential charge density analysis (Figs. 10c and S12 (online)). The negatively charged Pd-Cu_2O interface as the active place absorb the glucose molecules with the positive

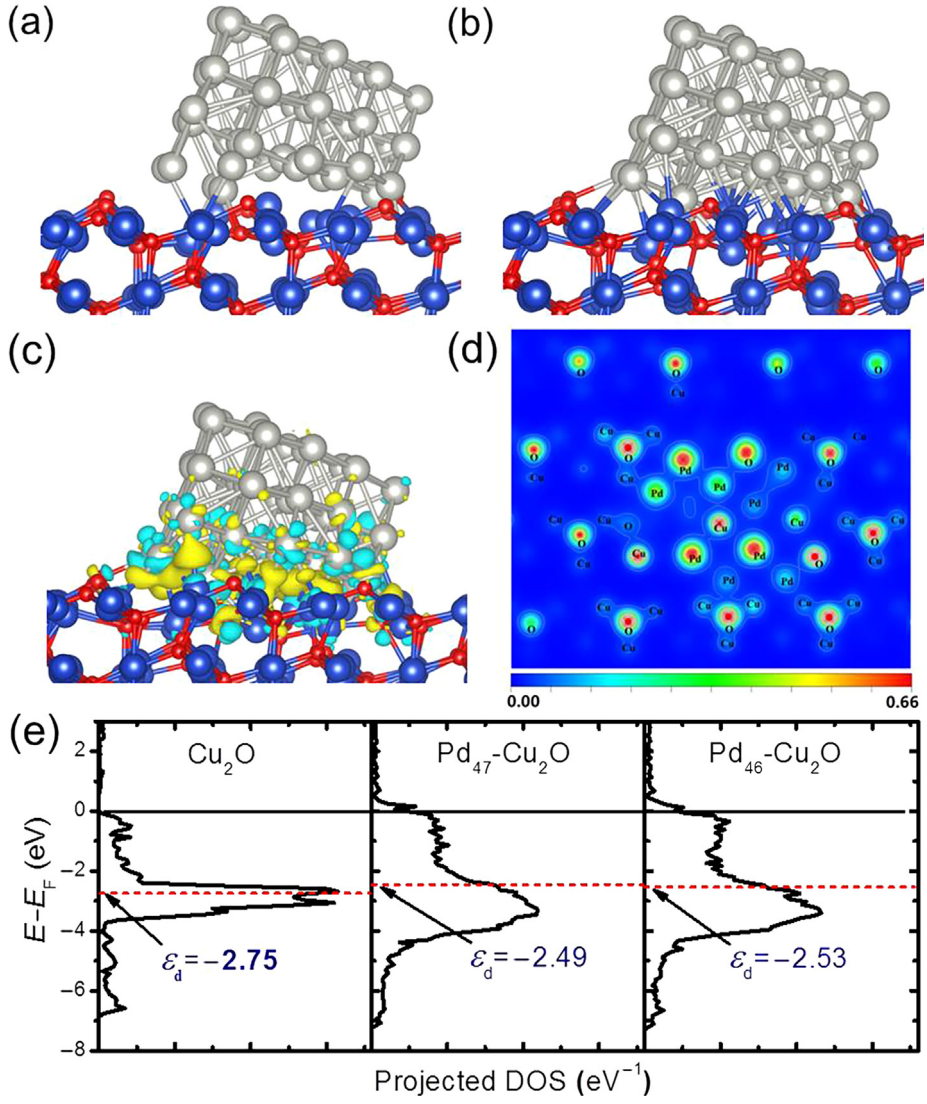

Fig. 10. (Color online) DFT calculations on Pd-Cu_2O nanoheterostructures. Optimized Pd_{47} (a) and Pd_{46} (b) cluster on Cu_2O(1 1 1), modeling the interface of Pd(3 1 0)-Cu_2O (1 1 1). (c) Differential charge density for the interface of Pd_{46}(3 1 0)-Cu_2O(1 1 1). (d) Charge density contour map for the middle plane between the Pd(3 1 0) and Cu_2O(1 1 1) surface for the Pd_{46}/Cu_2O(1 1 1) system. (e) Projected density of states (PDOS) for the Cu_2O(1 1 1), Pd_{47}-Cu_2O(1 1 1) and Pd_{46}-Cu_2O(1 1 1). The *d* band centers (ε_d) are calculated for Cu (Cu_2O), Cu and Pd (for Pd_{47}-Cu_2O and Pd_{46}-Cu_2O), respectively.

charged H and thus facilitate the electrochemical oxidation of glucose (Fig. S13 online). Accordingly, the charge density near the interface on both the Pd and Cu_2O sides decrease (Fig. 10c), indicating that the formation of interfacial Pd-O and Pd-Cu bonds is responsible for the donation of electrons from nearby Pd and Cu atoms. The charge analysis was also performed to discover the electron transfer. Net electron transfer neither from Pd to Cu_2O nor from Cu_2O to Pd was not observed. However, from the charge density contour shown in Fig. 10d, it is found that charge density of the junction area increase significantly, confirming the strong junction between Pd(3 1 0) and Cu_2O(1 1 1) surface and the electron accumulation at the interface.

4. Conclusions

Pd nanoparticles were deposited onto Cu_2O by non-epitaxial growth method, and the resulting nanoheterostructures deliver a high electrocatalytic activity toward the glucose oxidation and have a promising potential for practical application of glucose detection. Based on experimental characterizations, mathematical deduction and DFT calculations, Pd(3 1 0) facets are identified to exert a strong metal-oxide interface interaction with Cu_2O(1 1 1) facets, which arises from their lattice mismatch. This leads to the sinking of O atoms and protruding of Cu atoms of Cu_2O, and the Pd dislocations and vacancies, which facilitate the formation stable interfacial bonds between Pd and Cu_2O. Such interaction induced electron accumulation at the interface of Pd(3 1 0) and Cu_2O(1 1 1), which was further confirmed by the shifting up of *d* bands center of Cu-Pd toward the Fermi level. This work finds a novel metal-oxide interfacial effect of Pd-Cu_2O nanoheterostructures caused by crystalline imperfections and electron accumulation, which provides a new route to design and develop high-performance electrocatalysts via the interaction of mismatched facets.

Conflict of interest

The authors declare that they have no conflict of interest.

Acknowledgments

This work was supported by the National Natural Science Foundation of China (21203236), Guangdong Department of Science and Technology (2017A050501052), and Shenzhen Research Plan (JCYJ20160229195455154).

Author contributions

Ying Guo and Xian-Zhu Fu conceived and designed the experiments. Ying Guo performed all the experiments. Yi-Tao Xu and Bo Zhao carried out SEM measurements and analyzed the data. Jianwen Liu conducted all DFT modeling and calculations. Ying Guo, Jianwen Liu and Xian-Zhu Fu analyzed all data and wrote the paper. Rong Sun and Ching-Ping Wong discussed the results and commented on the manuscript. All authors contributed to the manuscript and the interpretation of the results.

Appendix A. Supplementary data

Supplementary data to this article can be found online at https://doi.org/10.1016/j.scib.2019.04.025.

References

[1] Chen G, Zhao Y, Fu G, et al. Interfacial effects in iron-nickel hydroxide–platinum nanoparticles enhance catalytic oxidation. Science 2014;344:495–9.
[2] van der Vliet DF, Wang C, Tripkovic D, et al. Mesostructured thin films as electrocatalysts with tunable composition and surface morphology. Nat Mater 2012;11:1051–8.
[3] Lin Y, Ren J, Qu X. Nano-gold as artificial enzymes: hidden talents. Adv Mater 2014;26:4200–17.
[4] Yehezkeli O, Tel-Vered R, Reichlin S, et al. Nano-engineered flavin-dependent glucose dehydrogenase/gold nanoparticle-modified electrodes for glucose sensing and biofuel cell applications. ACS Nano 2011;5:2385–91.
[5] Yamauchi Y, Tonegawa A, Komatsu M, et al. Electrochemical synthesis of mesoporous Pt-Au binary alloys with tunable compositions for enhancement of electrochemical Performance. J Am Chem Soc 2012;134:5100–9.
[6] Wang J. Electrochemical glucose biosensors. Chem Rev 2007;108:814–25.
[7] Dong XC, Xu H, Wang XW, et al. 3D graphene-cobalt oxide electrode for high-performance supercapacitor and enzymeless glucose detection. ACS Nano 2012;6:3206–13.
[8] Lang XY, Fu HY, Hou C, et al. Nanoporous gold supported cobalt oxide microelectrodes as high-performance electrochemical biosensors. Nat Commun 2013;4:2169–77.
[9] Yu R, Pan C, Chen J, et al. Enhanced performance of a ZnO nanowire-based self-powered glucose sensor by piezotronic effect. Adv Funct Mater 2013;23:5868–74.
[10] Bao SJ, Li CM, Zang JF, et al. New nanostructured TiO_2 for direct electrochemistry and glucose sensor applications. Adv Funct Mater 2008;18:591–9.
[11] Pan JH, Wang XZ, Huang Q, et al. Large-scale synthesis of urchin-like mesoporous TiO_2 hollow spheres by targeted etching and their photoelectrochemical properties. Adv Funct Mater 2014;24:95–104.
[12] Lee Y, Garcia MA, Frey Huls NA, et al. Synthetic tuning of the catalytic properties of Au-Fe_3O_4 nanoparticles. Angew Chem Int Ed 2010;122:1293–6.
[13] Tauster SJ. Strong metal-support interactions. Acc Chem Res 1987;20:389–94.
[14] Shoaib A, Ji M, Qian H, et al. Noble metal nanoclusters and their in situ calcination to nanocrystals: precise control of their size and interface with TiO_2 nanosheets and their versatile catalysis applications. Nano Res 2016;9:1763–74.
[15] Tao L, Shi Y, Huang YC, et al. Interface engineering of Pt and CeO_2 nanorods with unique interaction for methanol oxidation. Nano Energy 2018;53:604–12.
[16] Zhang Y, Shi Y, Chen R, et al. Enriched nucleation sites for Pt deposition on ultrathin WO_3 nanosheets with unique interactions for methanol oxidation. J Mater Chem A 2018;6:23028–33.
[17] Fu Q, Yang F, Bao X. Interface-confined oxide nanostructures for catalytic oxidation reactions. Acc Chem Res 2013;46:1692–701.
[18] Weng Z, Liu W, Yin LC, et al. Metal/oxide interface nanostructures generated by surface segregation for electrocatalysis. Nano Lett 2015;15:7704–10.
[19] Tauster SJ, Fung SC, Baker RTK, et al. Strong interactions in supported-metal catalysts. Science 1981;211:1121–5.
[20] Hu P, Huang Z, Amghouz Z, et al. Electronic metal-support interactions in single-atom catalysts. Angew Chem Int Ed 2014;53:3418–21.
[21] Lin L, Zhou W, Gao R, et al. Low-temperature hydrogen production from water and methanol using Pt/α-MoC catalysts. Nature 2017;544:80–3.
[22] Gao D, Zhang Y, Zhou Z, et al. Enhancing CO_2 electroreduction with the metal-oxide interface. J Am Chem Soc 2017;139:5652–5.
[23] Tauster SJ, Fung SC, Garten RL. Strong metal-support interactions. Group 8 noble metals supported on titanium dioxide. J Am Chem Soc 1978;100:170–5.
[24] Matthey D, Wang JG, Wendt S, et al. Enhanced bonding of gold nanoparticles on oxidized TiO_2(110). Science 2007;315:1692.
[25] Vayssilov GN, Lykhach Y, Migani A, et al. Support nanostructure boosts oxygen transfer to catalytically active platinum nanoparticles. Nat Mater 2011;10:310–5.
[26] Matsubu JC, Zhang S, DeRita L, et al. Adsorbate-mediated strong metal–support interactions in oxide-supported Rh catalysts. Nat Chem 2017;9:120–7.
[27] Lykhach Y, Kozlov SM, Skala T, et al. Counting electrons on supported nanoparticles. Nat Mater 2016;15:284–8.
[28] Cargnello M, Doan Nguyen VVT, Gordon TR, et al. Control of metal nanocrystal size reveals metal-support interface role for ceria catalysts. Science 2013;341:771.
[29] Kim SM, Lee H, Park JY. Charge transport in metal-oxide interfaces: genesis and detection of Hot electron flow and its role in heterogeneous catalysis. Catal Lett 2015;145:299–308.
[30] Chen G, Xu C, Huang X, et al. Interfacial electronic effects control the reaction selectivity of platinum catalysts. Nat Mater 2016;15:564–9.
[31] Wang YG, Yoon Y, Glezakou VA, et al. The role of reducible oxide-metal cluster charge transfer in catalytic processes: new insights on the catalytic mechanism of CO oxidation on Au/TiO_2 from ab initio molecular dynamics. J Am Chem Soc 2013;135:10673–83.
[32] Li L, Chen X, Wu Y, et al. Pd-Cu_2O and Ag-Cu_2O hybrid concave nanomaterials for an effective synergistic catalyst. Angew Chem Int Ed 2013;52:11049–53.
[33] Zhang Z, Xu B, Wang X. Engineering nanointerfaces for nanocatalysis. Chem Soc Rev 2014;43:7870–86.
[34] Fu Q, Li WX, Yao Y, et al. Interface-confined ferrous centers for catalytic oxidation. Science 2010;328:1141.
[35] Wang L, Ge J, Wang A, et al. Designing p-type semiconductor-metal hybrid structures for improved photocatalysis. Angew Chem Int Ed 2014;126:5207–11.
[36] Farmer JA, Campbell CT. Ceria maintains smaller metal catalyst particles by strong metal-support bonding. Science 2010;329:933.

[37] Lin P, Chen X, Yan X, et al. Enhanced photoresponse of Cu_2O/ZnO heterojunction with piezo-modulated interface engineering. Nano Res 2014;7:860–8.
[38] Zhang J, Tang Y, Lee K, et al. Nonepitaxial growth of hybrid core-shell nanostructures with large lattice mismatches. Science 2010;327:1634.
[39] Jia W, Wu Y, Chen Y, et al. Interface-induced formation of onion-like alloy nanocrystals by defects engineering. Nano Res 2016;9:584–92.
[40] Gong J, Zhou F, Li Z, et al. Controlled synthesis of non-epitaxially grown Pd@Ag core-shell nanocrystals of interesting optical performance. Chem Commun 2013;49:4379–81.
[41] Tian N, Zhou ZY, Sun SG, et al. Synthesis of tetrahexahedral platinum nanocrystals with high-index facets and high electro-oxidation activity. Science 2007;316:732.
[42] Gai Boyes PL. Defects in oxide catalysts: fundamental studies of catalysis in action. Catal Rev 1992;34:1–54.
[43] Sheng J, Kang J, Ye H, et al. Porous octahedral PdCu nanocages as highly efficient electrocatalysts for the methanol oxidation reaction. J Mater Chem A 2018;6:3906–12.
[44] Xia X, Wang Y, Ruditskiy A, et al. 25th anniversary article: galvanic replacement: a simple and versatile route to hollow nanostructures with tunable and well-controlled properties. Adv Mater 2013;25:6313–33.
[45] Liu M, Liu R, Chen W. Graphene wrapped Cu_2O nanocubes: non-enzymatic electrochemical sensors for the detection of glucose and hydrogen peroxide with enhanced stability. Biosens Bioelectron 2013;45:206–12.
[46] Ji Y, Liu J, Liu X, et al. 3D porous Cu@Cu_2O films supported Pd nanoparticles for glucose electrocatalytic oxidation. Electrochim Acta 2017;248:299–306.

Ying Guo received his B.S. degree from Chongqing University and M.S. degree from Shenzhen Institutes of Advanced Technology, Chinese Academy of Sciences. Now he is a Ph.D. candidate in City University of Hong Kong. His research focuses on the nanostructured materials and novel materials and their applications for electrocatalysis and energy storage and conversion.

Xian-Zhu Fu received his Ph.D. degree in Chemistry from Xiamen University in 2007. After postdoctoral stay at University of Alberta in Canada, he joined the Shenzhen Institutes of Advanced Technology, Chinese Academy of Sciences. He is currently a full Professor in the College of Materials Science and Engineering, Shenzhen University. His research interests focus on electrochemistry and energy materials.

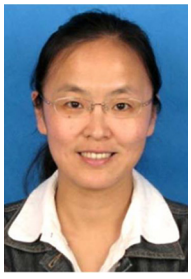

Rong Sun is a Professor at Shenzhen Institutes of Advanced Technology (SIAT), Chinese Academy of Sciences. She is also the director of Center for Advanced Materials and the deputy director of Institute of Advanced Integration Technology at SIAT. She received her Ph.D. degree from Lanzhou Institute of Chemical Physics, Chinese Academy of Sciences. Her research interests include electronic packaging materials and energy storage materials.